HHS Public Access

Author manuscript

*J Bone Miner Res*. Author manuscript; available in PMC 2018 August 01.

Published in final edited form as:

*J Bone Miner Res*. 2017 August ; 32(8): 1703–1715. doi:10.1002/jbmr.3165.

# Intermittent Parathyroid Hormone after Prolonged Alendronate Treatment Induces Substantial New Bone Formation and Increases Bone Tissue Heterogeneity in Ovariectomized Rats

**Allison R. Altman-Singles**[1,2], **Yonghoon Jeong**[3], **Wei-Ju Tseng**[1], **Chantal M. J. de Bakker**[1], **Hongbo Zhao**[1,4], **Carina Lott**[1], **Juhanna Robberts**[1], **Ling Qin**[1], **Lin Han**[5], **Do-Gyoon Kim**[3], and **X. Sherry Liu**[1,*]

[1]McKay Orthopaedic Research Laboratory, Department of Orthopaedic Surgery, Perelman School of Medicine, University of Pennsylvania, Philadelphia, PA, USA

[2]Pennsylvania State University, Berks Campus, Reading, PA, USA

[3]College of Dentistry, Division of Orthodontics, The Ohio State University, Columbus, OH, USA

[4]Key Laboratory of Biorheological Science and Technology, Ministry of Education and Bioengineering College, Chongqing University, Chongqing, China

[5]School of Biomedical Engineering, Science, and Health Systems, Drexel University, Philadelphia, PA, USA

## Abstract

Postmenopausal osteoporosis is often treated with bisphosphonates (e.g. alendronate, ALN), but over-suppression of bone turnover by long-term bisphosphonate treatment may decrease bone tissue heterogeneity. Thus, alternate treatment strategies after long-term bisphosphonates are of great clinical interest. The objective of the current study is to determine the effect of intermittent parathyroid hormone (PTH) following 12 weeks of alendronate (ALN, a bisphosphonate) treatment in 6-month-old, ovariectomized (OVX) rats on bone microarchitecture, bone remodeling dynamics, and bone mechanical properties at multiple length scales. By using *in vivo* μCT and 3D *in vivo* dynamic bone histomorphometry techniques, we demonstrated the efficacy of PTH following ALN therapy for stimulating new bone formation, and increasing trabecular thickness and bone volume fraction. In healthy bone, resorption and formation are coupled and balanced to sustain bone mass. OVX results in resorption outpacing formation, and subsequent bone loss and reduction in bone tissue modulus and tissue heterogeneity. We showed that ALN treatment effectively reduced bone resorption activity and regained the balance with bone formation,

*To whom correspondence should be addressed: X. Sherry Liu, McKay Orthopaedic Research Laboratory, Department of Orthopaedic Surgery, University of Pennsylvania, 426C Stemmler Hall, 36th Street and Hamilton Walk, Philadelphia, PA 19104, USA, xiaoweil@mail.med.upenn.edu, Phone: 1-215-746-4668.

**Conflict of Interest:**
No authors have conflicts of interest or disclosures to report

**Authors' roles:** Study design: XSL, ARA, LQ, LH, DGK. Study conduct: ARA, YJ, WJT, CMJdB, HZ, CL, JR. Data collection: ARA, YJ, WJT, CMJdB, HZ, CL, JR. Data analysis: ARA, TJ, WJT. Data interpretation: XSL, ARA, LH, LQ, DGK. Drafting manuscript: XSL. Revising manuscript content: ARA, YJ, WJT, CMJdB, CL, JR, LQ, LH, DGK. Approving final version of manuscript: XSL, ARA, YJ, WJT, CMJdB, HZ, CL, JR, LQ, LH, DGK. ARA and XSL take responsibility for the integrity of the data analysis.

preventing additional bone loss. However, ALN treatment also resulted in significant reductions in the heterogeneity of bone tissue mineral density and tissue modulus. On the other hand, PTH treatment was able to shift the bone remodeling balance in favor of formation, with or without a prior treatment with ALN. Moreover, by altering the tissue mineralization, PTH alleviated the reduction in heterogeneity of tissue material properties induced by prolonged ALN treatment. Furthermore, switching to PTH treatment from ALN improved bone's post-yield mechanical properties at both the whole bone and apparent level compared to ALN alone. The current findings suggest that intermittent PTH treatment should be considered as a viable treatment option for patients with prior treatment of bisphosphonates.

**Keywords**

Parathyroid hormone; bisphosphonates; bone formation; bone tissue material properties; bone microarchitecture

## 1. Introduction

Bisphosphonates are an osteoporosis treatment that acts to prevent bone loss by inhibiting bone resorption [(1)]. Bisphosphonates are among the most commonly prescribed drugs to reduce bone loss, and their efficacy to prevent fractures has been demonstrated in postmenopausal women and men with osteoporosis [(2)]. However, recently, compelling evidence indicates an association between bisphosphonate use and atypical subtrochanteric and femoral shaft fractures [(3,4)]. While incidence of atypical fractures is low, it occurs most often in patients who are exposed to long-term bisphosphonate treatment (median treatment 7 years) [(3,4)]. To date, the pathogenesis of atypical fractures remains unclear, and a causal link between bisphosphonate use and atypical fractures has not yet been established. Nevertheless, it is suspected that prolonged suppression of bone resorption may lead to advanced tissue age, microdamage accumulation, and decreased tissue heterogeneity [(3,5,6)]. Thus, alternate treatment strategies after long-term bisphosphonates are of great clinical interest.

Recombinant human parathyroid hormone (rhPTH) 1-34 is currently the only FDA-approved anabolic agent for osteoporosis when administered intermittently. Its mechanism of action is to promote bone remodeling and to shift the balance of remodeling towards increased bone formation [(7–9)]. As a result of its anabolic action, PTH may be able to replace the bone matrix of increased tissue age caused by bisphosphonates and stimulate new bone formation on resorption-suppressed bone surfaces [(10)]. However, early studies showed that combining PTH and bisphosphonates blunted the increase in areal bone mineral density (aBMD) compared with PTH alone, challenging the efficacy of PTH to initiate new bone formation on resorption-suppressed bone surfaces [(11–13)]. Since then, several studies have been conducted in order to elucidate the effect and associated mechanisms of PTH treatment on stimulating resorption-independent bone formation, also called modeling-based bone formation [(14–20)]. A number of studies suggested a positive effect of combined or tandem bisphosphonate and PTH therapies, attesting to PTH's anabolic effect in the absence of resorption [(21–28)]. In our previous studies, we developed a set of *in vivo* imaging techniques

that can assess bone formation and resorption activities simultaneously and longitudinally [29–32]. By applying these techniques to 3-month-old, intact female rats we demonstrated an additive effect by combined PTH and alendronate (ALN, a bisphosphonate) treatments on bone microarchitecture and stiffness over either monotherapy [29,30]. Therefore, we hypothesized that PTH is able to act through both resorption-dependent and -independent pathways to promote new bone formation after prolonged bisphosphonate treatment. Moreover, we expected that the stimulated new bone formation would help to reduce the tissue age and increase the tissue heterogeneity.

The objective of the current study is to determine the effect of intermittent PTH following 12 weeks of alendronate treatment on bone microarchitecture, bone remodeling dynamics, and bone tissue material quality in 6-month-old, ovariectomized (OVX) rats. Advanced *in vivo* imaging techniques allow us to monitor longitudinal changes in bone microarchitecture and examine the balance between bone resorption and formation at the highest spatial and temporal resolutions. Moreover, nanoindentation tests enable the measurement of intrinsic bone tissue mechanical properties. We hypothesized that PTH after prolonged ALN treatment can efficiently stimulate new bone formation, alleviating reductions in bone tissue heterogeneity induced by ALN, and improving bone mass, bone microarchitecture, and mechanical properties.

## 2. Materials and Methods

### 2.1 Animals and treatment plans

All experiments were approved by the University of Pennsylvania's Institutional Animal Care and Use Committee. A total of 30 female Sprague Dawley rats were purchased (Charles River) and received surgery at 4 months of age: 24 received a bilateral ovariectomy (OVX) surgery, and 6 received a sham OVX surgery. The study began when all rats were 6 months old, after an 8-week development of osteoporosis in the OVX rats. The treatment plan consisted of 2 phases, covering a total of 16 weeks (Phase 1: Week 0 to Week 12; and Phase 2: Week 12 to Week 16, Figure 1). The SHAM rats served as a control group (n=6) without receiving any treatment. The OVX rats were assigned to 4 groups (n=6/group): (1) a vehicle (VEH) group receiving subcutaneous saline injections 2 times a week during Phase 1 and 5 times a week during Phase 2; (2) an ALN group receiving subcutaneous ALN injections (alendronate sodium trihydrate, 28μg/kg, Sigma Aldrich, St. Louis, MO) twice per week during both Phase 1 and Phase 2, (3) a VEH/PTH group treated with saline for Phase 1, then switched to subcutaneous injections of PTH (Human Recombinant PTH1-34, 40 μg/kg, Bachem, Bubendorf, Switzerland) during Phase 2, and (4) an ALN/PTH group treated with ALN for Phase 1, then switched to PTH for Phase 2 (Figure 1). Rats were randomly assigned to different groups, housed in standard conditions in groups of three rats per cage. Experiments were performed unblinded.

### 2.2 In vivo μCT scans, image registration, and trabecular bone microstructural analysis of the proximal tibia

The right proximal tibiae of all rats were scanned by μCT (vivaCT 40, Scanco Medical AG, Brüttisellen, Switzerland) at week 0 (8-week post OVX/Sham surgery), then weekly from

Week 11 to Week 16 (Figure 1). As described in [29] and [33], rats were anesthetized (4.0/2% isoflurane), and the right leg of each rat was inserted into a custom holder to ensure minimal movement during the scan. A 4 mm region of the tibia, distal to the proximal growth plate, was scanned at 10.5 μm voxel size, 55 kVp energy, 145 μA intensity, 200 ms integration time, and 1000 projections, using a 0.5mm Al filter and a standard, manufacturer-provided beam-hardening correction algorithm, resulting in a total scan time of about 20 minutes and approximate radiation dose of 0.639 Gy per scan.

A landmark-initialized, mutual-information-based registration toolkit of an open source software (National Library of Medicine Insight Segmentation and Registration Toolkit, USA) was used to register the baseline and follow-up scans [34–36]. Briefly, by registering the unaltered trabecular patterns, the common region of trabecular bone volume can be located in each longitudinal μCT image so that the microstructural changes can be quantified at each time point within the same trabecular volume. The detailed methods have been published in our previous work [31]. The trabecular volume of interest (VOI) was defined through semi-automatic contouring of the trabecular bone compartment based on the Week 16 scan. The VOI chosen was approximately 2.6 mm distal from the growth plate and 200 slices corresponding to a 2.1 mm thick section of the trabecular compartment in the Week 16 scan. Transformation matrices from the registrations were then applied to this VOI to locate the corresponding volume of trabecular bone in images from previous time points. Representative baseline and registered follow-up images of each treatment group are shown in Figure 2.

Bone voxels of each registered image were segmented from the bone marrow and background using Gaussian filtering (sigma=1.2 and support=2.0) and a global threshold corresponding to 476 mgHA/cm$^3$. This threshold was determined by an adaptive threshold function provided by the μCT image analysis software on a subset of baseline images, and averaged to be used for all subsequent analyses. Bone microstructural parameters including bone volume fraction (BV/TV), trabecular thickness (Tb.Th), trabecular spacing (Tb.Sp), trabecular number (Tb.N), structure model index (SMI), and connectivity density (Conn.D), were evaluated for registered VOIs of weeks 0, 12, 14, and 16.

### 2.3 3D in vivo dynamic bone histomorphometry measurements

A 3D, *in vivo* dynamic bone histomorphometry technique was developed to track bone resorption and formation activities [30,32]. A trabecular bone sub-volume (1.575x1.575x1.05mm$^3$) of each week in Phase 2 (weeks 12–16) was subtracted from the registered sub-volume of the previous week (weeks 11–15) by comparing two subsequent, registered scans. The bone voxels that exist in the 2$^{nd}$ scan but don't exist in the 1$^{st}$ scan were defined as new bone formation (green, Figure 2 Right), while the bone voxels that exist in the 1$^{st}$ scan but not in the 2$^{nd}$ scan were defined as resorption (red, Figure 2 Right). The resulting image was then used to obtain 3D measurements of the volume, thickness, and surface area of bone formation and resorption sites. Measurements of bone formation and resorption, including bone formation rate (BFR/BS), mineralizing surface (MS/BS), resorption rate (BRR/BS), and erosion surface (ES/BS) were made analogously to standard dynamic bone histomorphometry. This method has been validated through comparison to

analogous histology-derived measures [30]. Significant correlations were found for μCT- and histology-based BFR/BS (r=0.83), and between BRR/BS and serum TRAP, a bone resorption marker (BRR/BS not quantifiable in histology, r=0.94) [30].

### 2.4 2D Static Bone Histomorphometry and Serum Biochemistry Analysis

After euthanasia, the right tibia was harvested immediately for methylmethacrylate (MMA) embedding. Five-μm-thick longitudinal sections were cut using a Polycut-S motorized microtome (Reichert, Heidelberg, Germany) for static measurements. Static histomorphometry slices were stained with Goldner's trichrome to identify osteoclasts, osteoblasts, and bone surface. All histomorphometric measurements were performed in an area 2.0–5.0 mm below the growth plate using Bioquant Osteo Software (Bioquant Image Analysis, Nashville, TN) and the following parameters were derived: osteoblast and osteoclast number per bone surface (Ob.N/BS and Oc.N/BS, 1/mm), and the percentage of osteoblast and osteoclast surface (Ob.S/BS and Oc.S/BS, %) [37]. Blood was collected via cardiac puncture at the time of euthanasia and left at room temperature for 30 min before being placed on ice and centrifuged at 2000×g for 10 min to separate sera. Serum TRACP 5b levels were determined by the RatTRAP™ Assay (Immunodiagnostic Systems, Scottsdale, AZ).

Linear regression analyses were performed to evaluate the correlations between 3D *in vivo* bone dynamic histomorphometry parameters (BFR/BS, BRR/BS) and parameters derived from 2D static bone histomorphometry and serum analysis (Ob.N/BS, Ob.S/BS, Oc.N/BS, Oc.S/BS, and TRAP).

### 2.5 Microstructure and Tissue Mineral Density (TMD) Analysis for the Lumbar Vertebra L2

After euthanasia, the lumbar vertebra L2 was dissected and a total of 600 slices corresponding to a 2.1 mm region of the center of L2 were scanned by μCT (Scanco microCT 35) at 3.5 μm voxel size. A 1.05x1.05x1.05 $mm^3$ cubic sub-volume was extracted from the center of the trabecular compartment for tissue mineral density (TMD) analysis. TMD reflects the tissue-level characterization of bone matrix mineralization. To assess TMD, μCT attenuation values were first converted to hydroxyapatite density (mg HA/$cm^3$) using a linear conversion calibrated by a phantom. By digital topological analysis (DTA)-based skeletonization [38,39], trabecular bone voxels were iteratively peeled off layer-by-layer for 4 layers without altering the shape or topology of the trabecular microarchitecture [38–40]. Then, the first, outer-most layer of bone surface, which might be affected by partial volume effect, was discarded. The $2^{nd}$-$4^{th}$ bone layers were defined as the surface trabecular bone tissue. The voxels greater than 4 layers from the surface were defined as the central trabecular bone tissue. Surface bone tissue mineral density (sTMD) and central bone tissue mineral density (cTMD), were calculated as the total bone mineral content within each envelope divided by volume of the envelope. Moreover, a TMD ratio, defined as TMDc/TMDs, was calculated to reflect the heterogeneity of TMD distribution within the bone tissue.

For trabecular bone microstructure analysis, images were downsampled to 7 μm voxel size and the trabecular compartment was isolated and subjected to analyses for BV/TV, Tb.N, Tb.Th, Tb.Sp, SMI, and Conn.D.

### 2.6 Cortical Bone Analysis and 3-Point Bending Test of Femoral Shaft

The right femur was dissected after euthanasia. A 2.3 mm region of femur midshaft was scanned by μCT (Scanco vivaCT 40) at 10.5 μm image voxel size. Standard cortical parameters including cortical thickness (Ct.Th), cortical porosity (Ct.Po), cortical tissue mineral density (Ct.TMD), polar moment of inertia (pMOI), periosteal perimeter (Ct.Pe.Pm), and endosteal perimeter (Ct.En.Pm) were evaluated for a 0.53 mm thick region in the center of the midshaft. A destructive 3-point bending test was then performed at the midshaft region with a displacement rate of 1.8 mm/min and a span length of 10 mm (Instron 5542, Norwood, MA). The load-displacement curve was used to calculate stiffness, peak load, and energy to failure. Then, the μCT-derived moment of inertia and bone area were used to estimate Young's modulus, ultimate stress, energy to failure, and post-yield energy to failure [41].

### 2.7 Uniaxial Compression Tests for the Lumbar Vertebra L1

After euthanasia, the first lumbar vertebra (L1) was harvested. The vertebra body was cut at both ends of the growth plate using a low speed diamond saw (IsoMet, Buehler) with water irrigation. A ~4-mm specimen with two paralleled endplates was then obtained for the uniaxial compression test. The detailed sample preparation method can be found in [42]. The uniaxial compression test was performed in a displacement control with a speed of 0.03mm/s using an Instron 5542 universal testing system (Instron, Norwood, MA). The specimen was compressed between two concentric cylindrical plates under room temperature. A preloading of 10N was applied before the test to prevent the addition of vibration at the beginning of the test. The load force and extension data were collected during the whole test. The load-displacement curve was used to calculate stiffness, peak load, energy to failure, and post-yield energy to failure. Then, μCT-derived cross-sectional area (CSA) of L1 was used to estimate Young's modulus, ultimate stress, energy to failure, and post-yield energy to failure.

### 2.8 Nanoindentation Tests for the Lumbar Vertebra L2

Following the μCT imaging analyses, L2 was sectioned along the transverse plane by a low speed diamond saw under water irrigation. The dissected surface of specimens were polished using silicon carbide abrasive papers with decreasing grit sizes (1200, 2400, and 4000 grits) and $Al_2O_3$ pastes (1 and 0.3 μm) on soft polishing cloths in wet conditions. Sonication of the specimen in de-ionized water followed to remove debris. Then, the unpolished surface of the specimen was glued onto a polycarbonate holder with a fluid drainage system in a nanoindenter (Nano-XP, MTS, Oakridge, TN) as described in previous studies [43–45]. All specimens were hydrated during nanoindentation. Central (C, center of a trabecula) and surface (S, ~10 μm from the edge of a trabecula) regions of individual trabecular bone structures were identified using a light microscope incorporated within the nanoindenter and 15 indents were made for those regions of each specimen using a pyramidal Berkovich tip of the nanoindenter. All specimens were hydrated during

nanoindentation. An indentation load rate corresponding to a displacement rate of 10 nm/sec was applied up to a 500 nm indentation depth. Following the 30-second holding period, the indenter was unloaded with the same rate. Using the slope of the unloading force-displacement curve, nanoindentation elastic moduli for the inner trabecular region (Ec) and the surface (Es) were measured following the Oliver-Pharr method [46]. Coefficient of variance (Ecv) was calculated for each treatment group to examine the heterogeneity of elastic modulus. Data of all samples within each group were pooled for comparisons in Ec, Es and Ecv between groups. Lastly, linear correlations between Es and TMDs, and between TMDc and Ec were evaluated.

### 2.9 Statistical Analysis

All statistical analyses were performed using NCSS 7.1.14 (NCSS, LLC, Kaysville, UT). Mean ± standard deviation (SD) are given for all the results. For longitudinal μCT image-based measurements, a two-way, repeated measures ANOVA was used to compare treatment groups over time. All comparisons were adjusted for baseline measures. In the presence of statistically significant main effects of time, treatment, and treatment*time interactions, *post-hoc* comparisons of between-group differences at each time point and within-group differences between different time points were made using a Bonferroni correction. A one-way ANOVA with a Bonferroni *post hoc* test was performed to determine the treatment effect on femoral cortical bone, vertebral trabecular bone, serum markers, bone static and dynamic parameters, TMD and indentation moduli measured at the end of treatment. Bartlett's test with a Bonferroni correction was used to compare the variance of indentation moduli between treatment groups. For all analyses, a two-tailed $p \leq 0.05$ was considered to indicate statistical significance.

## 3. Results

### 3.1 Longitudinal Changes in Trabecular Bone Microstructure at the Proximal Tibia

At baseline, rats in the SHAM group had an average BV/TV of 0.50 at the proximal tibia. In contrast, rats of the VEH, ALN, VEH/PTH, and ALN/PTH groups had an averaged BV/TV of 0.13 at baseline, resulting from the 8-week osteoporosis development post OVX surgery (Supplemental Table 1). During Treatment Phase 1, tibial BV/TV dropped 57% in rats of the VEH and VEH/PTH groups over 12 weeks. This bone loss was associated with a 47% decrease in Tb.N, 104% increase in Tb.Sp, and 79% decrease in Conn.D (Figure 3). Rats in the SHAM group also experienced an 11% bone loss in the proximal tibia, which was associated with 12% and 19% decreases in Tb.N and Conn.D, respectively, and an increase in SMI from -1.1 to 0. In contrast, ALN treatment effectively stabilized BV/TV for rat proximal tibia in the ALN and ALN/PTH groups, with no changes in any trabecular bone microarchitecture parameters (Figure 3).

During Phase 2, no significant change occurred in any trabecular bone parameters in the proximal tibia of SHAM, VEH, or ALN groups. In contrast, switching to PTH resulted in a 42% increase in BV/TV of the proximal tibia in the ALN/PTH group by week 16 (end of Phase 2) compared to week 12 (end of Phase 1). Changes in BV/TV in the VEH/PTH group (40%) did not reach statistical significance. Nevertheless, the change of BV/TV in

VEH/PTH group (40%) during Phase 2 was significantly greater than that in the VEH group (-23%). Moreover, Tb.Th of the proximal tibia in both VEH/PTH and ALN/PTH groups increased significantly (33% and 25%, respectively) in response to the 4-week PTH treatment during Phase 2 (Figure 3).

### 3.2 Cross-sectional Comparisons of Lumbar Spine and Femur Midshaft between Treatment Groups

At the end of Phase 2, BV/TV of the lumbar vertebra L2 of the VEH group was 38% lower than that of the SHAM group (Figure 4). Furthermore, rats in the VEH group had 20% lower Tb.N, 16% lower Tb.Th, 31% lower Conn.D, and 33% greater Tb.Sp than the SHAM group. The SMI of the L2 in the VEH group was also significantly higher than the SHAM group (0.5 vs. -0.3). Treatments of VEH/PTH, ALN, and ALN/PTH resulted in similar BV/TV that were significantly greater than BV/TV in the VEH group (38%, 37%, and 59%, respectively, Figure 4). The BV/TV of the L2 in all three treatment groups was not different from that in the SHAM group. However, the treatment effects on trabecular bone microarchitecture were different. Rats in the VEH/PTH group had greater Tb.Th and similar Tb.N, Tb.Sp, and Conn.D compared to VEH group while rats in the ALN group had greater Tb.N and Conn.D, lower Tb.Sp, but similar Tb.Th compared to the VEH group. ALN/PTH treatment had benefits from both ALN and PTH, resulting in similar bone microarchitecture in the L2 as the SHAM group, with even greater Tb.Th (Figure 4).

No difference was found between groups in the femur, including Ct.Th and all microstructural parameters as well as whole bone mechanical properties and derived tissue mechanical properties. Detailed results were reported in Supplemental Table 2.

### 3.3 2D Static Bone Histomorphometry and Serum Biochemistry Analysis

No difference was found in Ob.N/BS or Ob.S/BS of the proximal tibia between SHAM and VEH groups (Figure 5A & 5B). Vehicle-treated OVX rats (VEH group) had 159% greater Oc.N/BS and 195% greater Oc.S/BS than the SHAM group (Figure 5C & 5D). However, serum TRAP level was not different between SHAM and VEH groups (Figure 5E). PTH following VEH treatment (VEH/PTH group) resulted in significantly greater Ob.N/BS and Ob.S/BS compared to SHAM, VEH, or ALN groups. Similarly, PTH following ALN treatment (ALN/PTH group) resulted in greater Ob.N/BS than VEH and ALN groups, as well as greater Ob.S/BS than SHAM, VEH, and ALN groups. However, the Ob.N/BS and Ob.S/BS in ALN/PTH group were lower than those in VEH/PTH group. Compared to the VEH group, Oc.N/BS was 61% and 67% lower in the VEH/PTH and ALN/PTH groups, respectively, while Oc.S/BS was 55%, 51%, and 68% lower in the ALN, VEH/PTH, and ALN/PTH groups, respectively. Moreover, serum TRAP levels in the ALN, VEH/PTH, and ALN/PTH groups were 55%, 42%, and 43% lower than that in the VEH group, respectively.

### 3.4 3D In Vivo Dynamic Bone Histomorphometry Analysis

Comparisons between the rates of bone resorption (BRR/BS) and bone formation (BFR/BS) over the last week of Phase 2 (Figure 5F) demonstrated that SHAM and ALN groups had highly balanced bone remodeling dynamics, with similar BFR/BS and BRR/BS. In contrast, resorption outpaced formation by 139% for the VEH group. Furthermore, the balance

between bone resorption and formation was shifted in both VEH/PTH and ALN/PTH groups, but in a reversed manner compared to VEH group, as shown by a substantially greater BFR/BS than BRR/BS (468% and 346% in the VEH/PTH and ALN/PTH groups, respectively).

Linear correlation analysis showed that BFR/BS significantly correlated with Ob.S/BS ($r=0.73$, Figure 5G) and Ob.N/BS ($r=0.6$, Figure 5H). BRR/BS was significantly correlated with serum TRAP level ($r=0.74$, Figure 5I). However, no correlation was found for BRR/BS with Oc.S/BS or Oc.N/BS.

Longitudinal analyses of BFR/BS and BRR/BS over the course of Phase 2 revealed that VEH/PTH led to a dramatic increase in BFR/BS by week 13 and 14, which began to decrease at week 15 (Figure 6B). The BFR/BS did not change in the ALN/PTH group at week 13, but significantly increased by week 14, then remained elevated through week 16. At week 14 and 15, BFR/BS in the VEH/PTH group was greater than that in the ALN/PTH group. However, there was no remaining difference between these two groups at week 16. Both VEH/PTH and ALN/PTH groups had significantly greater BFR/BS than the VEH or ALN groups throughout weeks 14 to 16. Compared to BFR/BS, minimal changes were detected in BRR/BS over the Phase 2 in each treatment group (Figure 6E). The only significant change was found in the VEH/PTH group where BRR/BS at week 16 became lower than that at week 12. Moreover, at week 15 and 16, BRR/BS in the VEH group was significantly greater than all other groups. This result was consistent with those from static bone histomorphometry and serum TRAP analyses (Figure 5C–E).

### 3.5 Whole Bone and Apparent Mechanical Properties of the Lumbar Vertebra L1

At the whole bone level, significant differences were found in peak load, stiffness, energy to failure, and post-yield energy to failure between treatment groups (Figure 7A–D). Compared to the SHAM group, OVX (VEH group) resulted in 39% and 53% reduction in peak load and energy to failure, respectively. Compared to the VEH group, VEH/PTH led to 93% greater energy to failure and a trend of 45% greater peak load ($p<0.1$). ALN led to 20% greater energy to failure than the VEH group. ALN/PTH led to most significant treatment effect, resulting in 60%, 128%, and 96% greater peak load, energy to failure, and post-yield energy to failure, respectively, as compared to VEH. Moreover, ALN/PTH increased the post-yield energy to failure by 141% as compared to ALN alone.

There was no difference in the L1 cross-sectional bone area (Figure 7E). At the apparent level (after accounting for the CSA), significant treatment effects were found for ultimate stress, modulus of toughness and post-yield modulus of toughness (Figure 7F, H, and I) with no effect in elastic modulus (Figure 7G). Compared to the SHAM group, OVX (VEH group) resulted in 33% and 49% reductions in ultimate stress and toughness, respectively. Compared to the VEH group, no improvement was found by VEH/PTH or ALN, except for a trend of increase in toughness by VEH/PTH. In contrast, ALN/PTH led to 100% greater toughness, and a trend of increase in post-yield toughness as compared to VEH group. Moreover, compared to ALN alone, ALN/PTH increased the post-yield toughness by 140%.

### 3.6 Bone Tissue Mineral Density (TMD) and Tissue Elastic Modulus (E) of the Lumbar Vertebra L2

VEH/PTH, ALN, and ALN/PTH groups had 7%, 4%, and 5% lower TMDc than the SHAM group, respectively (Figure 8B). Compared to the VEH group, VEH/PTH lowered the TMDc by 4%. At the surface of the trabeculae, the VEH/PTH group had 5% and 6% lower TMDs than the SHAM and ALN groups, respectively (Figure 8C). ALN/PTH tended to lower TMDs as compared to the ALN treatment alone (4%, $p<0.1$).

Compared to the SHAM group, the VEH group had 11% lower modulus at the central region of the trabeculae (Ec, Figure 8E). ALN/PTH treatment resulted in 14% greater Ec than the VEH group. Ec in the ALN/PTH was also greater than that in the VEH/PTH group. For the Es, VEH and VEH/PTH groups were 13% and 10% lower than that of the SHAM group (Figure 8F). There was a trend towards an increased Es of the ALN group as compared to VEH (5%, $p<0.1$). Es of ALN/PTH group was not different from any other groups.

The Ecv in the VEH group was 12% lower than that in the SHAM group, indicating reduced heterogeneity in bone tissue material properties (Figure 8G). PTH treatment restored the heterogeneity as shown by a 10% greater Ecv in the PTH *vs.* VEH group. Moreover, ALN caused reduced heterogeneity in both bone tissue mineralization and material properties, as shown by a 23% lower Ecv and a 4% lower mineralization ratio (TMDc/TMDs) in ALN *vs.* the SHAM group (Figure 8D and 8G). ALN/PTH treatment was able to restore the heterogeneity demonstrated by a 31% greater Ecv and a trend toward 3% higher mineralization ratio ($p<0.1$) in ALN/PTH *vs.* ALN group.

Linear correlation analysis showed a significant correlation between TMD and E ($r=0.43$, $p=0.03$, Figure 8H). Further analysis suggested that TMDs was significantly correlated with Es ($r=0.58$, $p<0.01$, Figure 8I) but TMDc and Ec were not correlated (Figure 8J).

## Discussion

The results of this study clearly demonstrate the efficacy of PTH following bisphosphonate therapy for stimulating new bone formation. In healthy bone, resorption and formation are coupled and balanced to sustain bone mass. OVX results in resorption outpacing formation, and subsequent bone loss and reduction in bone tissue modulus and tissue heterogeneity. We showed that ALN treatment effectively regains this balance, preventing additional bone loss. However, ALN treatment also resulted in significant reductions in the heterogeneity of bone tissue mineral density and tissue modulus. On the other hand, PTH treatment was able to shift the bone remodeling balance in favor of formation, with or without a prior treatment with ALN. Moreover, by altering the tissue mineralization, PTH alleviated the reduction in heterogeneity of tissue material properties induced by prolonged ALN treatment. Furthermore, switching to PTH treatment from ALN improved bone's post-yield bone mechanical properties at both the whole bone and apparent level compared to ALN alone. The current findings suggest that intermittent PTH treatment should be considered as a viable treatment option for patients with prior treatment of bisphosphonates.

We used 6-month-old female rats that were induced to develop estrogen-deficiency induced osteoporosis by OVX surgery for 8 weeks. Before the treatment started, these rats had experienced rapid and significant bone loss that mimicked the onset of postmenopausal osteoporosis. During the 16 weeks of treatments, the vehicle-treated OVX rats continued to lose bone with a steady rate, serving as an ideal model to test the treatment efficacy to prevent or reverse continued osteoporosis development. In our study design, the Phase 2 consisted of only 4 weeks of PTH treatment. In clinical practice, the recommended duration of PTH treatment is 18–24 months [47], which corresponds to approximately 1 month in a rat's life span [48]. Since rodents have much faster bone turnover rate, a shorter treatment time in rats was selected to simulate the relatively short PTH treatment window in humans.

An advanced *in vivo* μCT imaging and image analysis technique was used in the current study. This technique allows the highest possible *in vivo* temporal and spatial resolution for longitudinal examination of changes in trabecular bone microarchitecture beyond bone mass. This experiment design also allows the highest precision in monitoring the relative change of each animal. As demonstrated in Figure 3, changes in the rat proximal tibia at the end of Phase 1 were highly consistent between VEH and VEH/PTH groups due to their same treatment regime of Phase 1. Similar consistency can be found for ALN and ALN/PTH groups. During the Phase 2 treatment, similar changes were found in VEH/PTH and ALN/PTH groups, suggesting that the anabolic effect of PTH treatment on rat tibial trabecular bone was not affected by prior treatment with ALN. Independent of prior treatments, PTH improved BV/TV by thickening the trabeculae, without changing the number, spacing, or connectivity of the trabecular network. This finding is consistent with what has been reported in our previous investigation in 3-month-old intact rats with 12-day PTH treatment [29]. In the current study, we did not observe any significant changes in SMI. However, in our previous study we observed a reduction in SMI by PTH treatment, suggesting a change toward more plate-like trabecular structure. A further study by individual trabecular dynamics (ITD) analysis suggested that this could be caused by targeted bone formation that fills the perforations on trabecular plates [49]. Although such a change was not detected in the current study by analysis using SMI, in our future studies we plan to perform more advanced analysis, such as ITD analysis, to examine the dynamics of conversions between trabecular rod-like and plate-like structures in the estrogen-deficient bone in response to different treatment regimes.

To address the concerns over PTH's efficacy to stimulate new bone formation on bone surfaces with suppressed resorption activities, detailed bone remodeling activities in response to various treatment regimes were examined. 3D *in vivo* dynamic bone histomorphometry analysis clearly demonstrated the shifts in bone resorption-formation balance following different therapies. Bone resorption and formation rates were well balanced in the SHAM. In contrast, BRR/BS in the VEH-treated OVX rats significantly outpaced BFR/BS. ALN treatment efficiently regained the balance between the BRR/BS and BFR/BS by lowering the BRR/BS, while VEH/PTH and ALN/PTH treatments significantly increased BFR/BS to outpace BRR/BS. Surprisingly, resorption activities in VEH/PTH rats were similar to those of the ALN group and remained significantly lower than those of the VEH and SHAM groups. This finding in rats was different from what has been reported in clinical studies. We expected that PTH treatment would increase bone turnover rate by

increasing both bone resorption and formation. Our previous studies in 1-month and 3-month old intact rats indicated significantly elevated osteoclast activities by intermittent PTH treatments. However, in the current study, data from three different analysis techniques, including static bone histomorphometry, serum resorption marker, and 3D *in vivo* bone dynamic histomorphometry, all indicated reduced bone resorption activities by VEH/PTH compared to VEH. The reason causing the discrepancy between the rat model and clinical findings is not clear. Previous clinical studies have shown a delay in the rise of bone resorption markers following that of the bone formation marker, thus providing an "anabolic window" that maximizes the short-term efficacy of PTH [(50)]. Our current study examined the effect of PTH treatment up to 4 weeks. We cannot exclude the possibility that a longer duration of PTH treatment is required to induce accelerated bone resorption in the rat model, which needs to be determined in future studies.

Results from both static and *in vivo* dynamic bone histomorphometry indicated marked increases in bone formation activities in VEH/PTH and ALN/PTH treated rats. Furthermore, the 3D *in vivo* dynamic bone histomorphometry analysis allowed us to monitor the week-by-week responses in BFR/BS to the 4-week PTH treatment. In the VEH/PTH group, BFR/BS had a rapid increase during the first 2 weeks of PTH treatment, then reached a plateau during the 3$^{rd}$ week, followed by a decrease in the 4$^{th}$ week. The rise of BFR/BS in the ALN/PTH group, on the other hand, had a 1-week delay compared to the VEH/PTH group, and was maintained during the 3$^{rd}$ and 4$^{th}$ weeks. Before the PTH treatment started (week 12), rats in the VEH/PTH group had greater bone resorption activities than those in the ALN/PTH group. Thus, we speculate that the faster rise of BFR/BS in the VEH/PTH group compared to the ALN/PTH group can be attributed to the enhanced bone formation at the existing bone resorption sites in the VEH/PTH group. PTH would be able to act on the pre-existing osteoblasts to accelerate their refilling the resorption cavity and "spill over" onto the adjacent bone surface to induce a positive bone balance [(8,20)]. Modeling-based bone formation may have a delayed response due to the time required for conversion of bone lining cells to osteoblasts [(10)]. This would explain the delay and the lower degree of increase in BFR/BS in response to ALN/PTH than to VEH/PTH treatment.

One of the advantages of the *in vivo* dynamic histomorphometry technique is its capability to evaluate bone resorption rate, which cannot be evaluated by traditional 2D dynamic histomorphometry. Our study showed consistent group comparison results in parameters associated with bone resorption activities among all OVX groups (VEH, VEH/PTH, ALN, ALN/PTH, Figure 5C–F). However, discrepancies were found when comparison was made between SHAM and VEH groups. While static histomorphometry indicated significantly increased Oc.N/BS and Oc.S/BS in the vehicle-treated OVX rats (VEH) compared to SHAM rats, serum TRAP5b level and BRR/BS by *in vivo* bone dynamics analysis did not differ between the two groups. Serum TRAP5b level reflects the total number of osteoclasts. Indeed, our results indicated a significant correlation between Oc.N and TRAP5b (data not shown). Moreover, without normalization by bone surface, Oc.N did not differ between VEH and SHAM groups. All the bone resorption analyses were made toward the end of the study (20–24 weeks after OVX surgery), which could partially explain the lack of difference in bone resorption activities between SHAM and OVX groups. Indeed, there was no significant change in BV/TV and other bone microstructure parameters in both the VEH and

SHAM groups during the last 4 weeks of the experiment (week 12–16, Figure 3 and Supplemental Table 1). On the other hand, BRR/BS is defined as the total amount of resorbed bone volume divided by bone surface and inter-scan duration, which is found to be significantly correlated with TRAP5b in the current study. Similarly, strong correlation (r=0.94) between BRR/BS and TRAP5b was also reported in our previous study in which 3-month-old intact rats were used [30]. Additionally, μCT-based BFR/BS and other bone formation parameters were also validated against the gold standard 2D dynamic histomorphometry based on calcein labels and strong correlations were found between the two techniques (r=0.72–0.83) [30].

Compared to the proximal tibia, the bone loss in the lumbar vertebra in response to estrogen deficiency was less severe. In the proximal tibia, treatment of ALN followed by PTH on the OVX rats helps to improve their bone mass and microarchitecture, but cannot revert them back to the same level as age-matched, sham operated rats (Supplemental Table 1). In contrast, ALN followed by PTH treatment helped to fully recover BV/TV, bone microarchitecture, and whole bone and apparent level mechanical properties in the lumbar vertebra of OVX rats to be comparable with those of SHAM rats. Our results suggested that continuous treatment of ALN alone was also sufficient for maintaining trabecular bone mass, microarchitecture, and whole bone and apparent mechanical properties at the lumbar vertebra. However, switching to PTH treatment from ALN led to a greater Tb.Th than ALN treatment alone, possibly caused by stimulation of new bone formation. Moreover, switching to PTH treatment from ALN improved the post-yield mechanical properties at both the whole bone and apparent level compared to ALN alone, as indicated by significantly increased post-yield energy to failure and post-yield toughness.

In addition to the benefit at the microstructural level, switching from ALN to PTH treatment also improve bone quality at the tissue level when compared to continuous ALN treatment. OVX-induced estrogen deficiency caused a significant reduction in the central and surface trabecular bone tissue moduli, as well as its heterogeneity. ALN-treated OVX rats, on the other hand, had significantly reduced heterogeneity of both tissue mineralization and tissue elastic modulus than those of SHAM rats. This finding was consistent with a previous clinical report which demonstrated reduced mineral and matrix heterogeneity in bisphosphonate-treated postmenopausal women [5]. Switching from ALN to PTH treatment led to a trend of reduced surface TMD and increase in the TMD heterogeneity, possibly associated with increases in under-mineralized osteoid through accelerated new bone formation. As a result, no difference in the heterogeneity of TMD or elastic modulus was found between ALN/PTH and SHAM groups. It is suggested that the reduction in bone tissue heterogeneity may lead to diminished tissue-level toughening mechanisms [51,52]. In the current study no change in bone toughness was found in ALN-treated bone as compared to the SHAM and VEH-treated bone. Nevertheless, we found a significant increase in post-yield bone toughness by ALN/PTH treatment as compared to ALN alone, suggesting that a follow-up treatment of PTH after a long-term bisphosphonate treatment may complement the anti-fracture efficacy of ALN treatment by improving bone tissue quality.

This study has several notable strengths and innovations. First, the *in vivo* μCT and 3D image registration techniques used in this study allowed accurate evaluation of the same

volume of interest (VOI) for each rat during the entire experiment, eliminating any confounding factors due to bone growth or changes in VOI. Second, 3D *in vivo* bone dynamic histomorphometry allowed simultaneous evaluation of bone resorption and formation in a longitudinal manner, thus providing additional insight into PTH's capability to stimulate new bone formation on resorption-suppressed bone surfaces. Third, both whole bone-scale (femur and lumbar vertebra) and nanoscale (vertebral trabecular bone) mechanical tests were performed to assess efficacy of various treatment regimes on bone mechanical properties. Despite these strengths, there are limitations associated with this study. First, different from clinical observations, multiple assays in the current study indicated a significant decrease in bone resorption activities in response to PTH treatment. A study with longer duration of PTH treatment is required to confirm whether the decrease in bone resorption is a transient response and will rise with prolonged treatment. Second, we have validated the μCT-based BRR/BS measurements by comparison with serum TRAP5b levels and demonstrated strong correlations between the two. It would be important in our future studies to validate μCT-based BRR/BS measurements by comparison with serum CTX levels. Direct validation against traditional bone histomorphometry is not available due to the difficulty to reliably identify the resorption surface on 2D bone sections. However, a novel 3D fluorescence imaging technique for measurement of individual resorption cavities and formation events was recently developed [53,54], which can be used to further validate the *in vivo* μCT-based bone resorption parameters. It should be noted that *in vivo* μCT causes localized ionizing radiation to the scanned bone region. However, several studies have suggested minimal effects of radiation associated with *in vivo* μCT on bone microstructure and cellular activities [55,56]. Moreover, all the treatment and control groups received the same exposure to *in vivo* μCT in our study. Therefore, we do not expect radiation effect of *in vivo* μCT impact our major conclusions. Third, we discovered a significant correlation between TMD and elastic modulus on the surface of trabeculae; however, no correlation was found in the center region of trabeculae. These results may suggest that during the mineralization process (bone surface), TMD is a primary determinant of material properties, but once mineralization is complete (bone center) TMD plays a lesser role. In addition to bone mineral crystals, bone tissue material properties are also determined by modifications in collagen quality, such as accumulated advanced glycation products, which has been reported to be associated with postmenopausal osteoporosis [57]. Further investigation is needed to examine other aspects of bone tissue quality for a better understanding of the mechanisms behind the observed differences in tissue material properties between different treatment regimes.

In summary, our investigation across multiple skeletal sites suggests that sequential treatment of ALN followed by PTH is a viable treatment strategy to maintain and improve bone quality by stimulating substantial new bone formation. The novel *in vivo* dynamic histomorphometry analysis provides direct evidence for PTH's anabolic effect in the absence of bone resorption, further confirming its capacity for modeling-based bone formation. Furthermore, by altering the tissue mineralization, PTH acts to alleviate the reductions in the heterogeneity of tissue mechanical properties induced by prolonged ALN treatment and further improve bone mechanical properties at both the whole bone and apparent level.

## Supplementary Material

Refer to Web version on PubMed Central for supplementary material.

## Acknowledgments

Research reported in this publication was supported by the Penn Center for Musculoskeletal Disorders (PCMD), NIH/NIAMS P30-AR050950, NIH/NIAMS K01-AR066743 (to XSL), University of Pennsylvania Institute on Aging (IOA) Pilot Award (to XSL), and National Science Foundation Graduate Research Fellowship (to CMJdB).

## References

1. Russell RG. Bisphosphonates: from bench to bedside. Annals of the New York Academy of Sciences. Apr.2006 1068:367–401. [PubMed: 16831938]
2. Eastell R, Walsh JS, Watts NB, Siris E. Bisphosphonates for postmenopausal osteoporosis. Bone. Jul; 2011 49(1):82–8. [PubMed: 21349354]
3. Shane E, Burr D, Ebeling PR, Abrahamsen B, Adler RA, Brown TD, et al. Atypical subtrochanteric and diaphyseal femoral fractures: report of a task force of the American Society for Bone and Mineral Research. J Bone Miner Res. Nov; 2014 25(11):2267–94.
4. Shane E, Burr D, Ebeling PR, Abrahamsen B, Adler RA, Brown TD, et al. Atypical subtrochanteric and diaphyseal femoral fractures: report of a task force of the American Society for Bone and Mineral Research. J Bone Miner Res. Nov; 2010 25(11):2267–94. [PubMed: 20842676]
5. Donnelly E, Meredith DS, Nguyen JT, Gladnick BP, Rebolledo BJ, Shaffer AD, et al. Reduced cortical bone compositional heterogeneity with bisphosphonate treatment in postmenopausal women with intertrochanteric and subtrochanteric fractures. J Bone Miner Res. Mar; 2012 27(3): 672–8. Epub 2011/11/11. [PubMed: 22072397]
6. Allen MR, Burr DB. Bisphosphonate effects on bone turnover, microdamage, and mechanical properties: what we think we know and what we know that we don't know. Bone. Jul; 2011 49(1): 56–65. Epub 2010/10/20. [PubMed: 20955825]
7. Qin L, Raggatt LJ, Partridge NC. Parathyroid hormone: a double-edged sword for bone metabolism. Trends in endocrinology and metabolism: TEM. Mar; 2004 15(2):60–5. [PubMed: 15036251]
8. Jilka RL. Molecular and cellular mechanisms of the anabolic effect of intermittent PTH. Bone. Jun; 2007 40(6):1434–46. [PubMed: 17517365]
9. Compston JE. Skeletal actions of intermittent parathyroid hormone: effects on bone remodelling and structure. Bone. Jun; 2007 40(6):1447–52. [PubMed: 17045858]
10. Kim SW, Pajevic PD, Selig M, Barry KJ, Yang JY, Shin CS, et al. Intermittent parathyroid hormone administration converts quiescent lining cells to active osteoblasts. J Bone Miner Res. Oct; 2012 27(10):2075–84. Epub 2012/05/25. [PubMed: 22623172]
11. Black DM, Greenspan SL, Ensrud KE, Palermo L, McGowan JA, Lang TF, et al. The effects of parathyroid hormone and alendronate alone or in combination in postmenopausal osteoporosis. N Engl J Med. Sep 25; 2003 349(13):1207–15. [PubMed: 14500804]
12. Finkelstein JS, Hayes A, Hunzelman JL, Wyland JJ, Lee H, Neer RM. The effects of parathyroid hormone, alendronate, or both in men with osteoporosis. N Engl J Med. Sep 25; 2003 349(13): 1216–26. [PubMed: 14500805]
13. Finkelstein JS, Wyland JJ, Lee H, Neer RM. Effects of teriparatide, alendronate, or both in women with postmenopausal osteoporosis. The Journal of clinical endocrinology and metabolism. Apr; 2010 95(4):1838–45. [PubMed: 20164296]
14. Erben RG. Trabecular and endocortical bone surfaces in the rat: modeling or remodeling? The Anatomical record. Sep; 1996 246(1):39–46. [PubMed: 8876822]
15. Kobayashi S, Takahashi HE, Ito A, Saito N, Nawata M, Horiuchi H, et al. Trabecular minimodeling in human iliac bone. Bone. Feb; 2003 32(2):163–9. [PubMed: 12633788]
16. Jee WS, Tian XY, Setterberg RB. Cancellous bone minimodeling-based formation: a Frost, Takahashi legacy. Journal of musculoskeletal & neuronal interactions. Jul-Sep;2007 7(3):232–9. [PubMed: 17947806]

17. Hodsman AB, Steer BM. Early histomorphometric changes in response to parathyroid hormone therapy in osteoporosis: evidence for de novo bone formation on quiescent cancellous surfaces. Bone. May-Jun;1993 14(3):523–7. [PubMed: 8363903]

18. Dempster DW, Cosman F, Kurland ES, Zhou H, Nieves J, Woelfert L, et al. Effects of daily treatment with parathyroid hormone on bone microarchitecture and turnover in patients with osteoporosis: a paired biopsy study. J Bone Miner Res. Oct; 2001 16(10):1846–53. [PubMed: 11585349]

19. Cusano NE, Bilezikian JP. Combination antiresorptive and osteoanabolic therapy for osteoporosis: we are not there yet. Current medical research and opinion. Sep; 2011 27(9):1705–7. [PubMed: 21740288]

20. Lindsay R, Cosman F, Zhou H, Bostrom MP, Shen VW, Cruz JD, et al. A novel tetracycline labeling schedule for longitudinal evaluation of the short-term effects of anabolic therapy with a single iliac crest bone biopsy: early actions of teriparatide. J Bone Miner Res. Mar; 2006 21(3): 366–73. [PubMed: 16491283]

21. Cosman F, Eriksen EF, Recknor C, Miller PD, Guanabens N, Kasperk C, et al. Effects of intravenous zoledronic acid plus subcutaneous teriparatide [rhPTH(1-34)] in postmenopausal osteoporosis. J Bone Miner Res. Mar; 2011 26(3):503–11. [PubMed: 20814967]

22. Cosman F, Keaveny TM, Kopperdahl D, Wermers RA, Wan X, Krohn KD, et al. Hip and spine strength effects of adding versus switching to teriparatide in postmenopausal women with osteoporosis treated with prior alendronate or raloxifene. J Bone Miner Res. Dec 21; 2013 28(6): 1328–36. [PubMed: 23281041]

23. Cosman F, Nieves JW, Zion M, Garrett P, Neubort S, Dempster D, et al. Daily or Cyclical Teriparatide Treatment in Women With Osteoporosis on no Prior Therapy and Women on Alendronate. The Journal of clinical endocrinology and metabolism. Jul; 2015 100(7):2769–76. Epub 2015/05/12. [PubMed: 25961136]

24. Schafer AL, Burghardt AJ, Sellmeyer DE, Palermo L, Shoback DM, Majumdar S, et al. Postmenopausal women treated with combination parathyroid hormone (1–84) and ibandronate demonstrate different microstructural changes at the radius vs. tibia: the PTH and Ibandronate Combination Study (PICS). Osteoporos Int. Oct; 2013 24(10):2591–601. [PubMed: 23589163]

25. Cosman F, Nieves J, Woelfert L, Shen V, Lindsay R. Alendronate does not block the anabolic effect of PTH in postmenopausal osteoporotic women. J Bone Miner Res. Jun; 1998 13(6):1051–5. Epub 1998/06/17. [PubMed: 9626638]

26. Stepan JJ, Burr DB, Li J, Ma YL, Petto H, Sipos A, et al. Histomorphometric changes by teriparatide in alendronate-pretreated women with osteoporosis. Osteoporos Int. Dec; 2010 21(12): 2027–36. Epub 2010/02/06. [PubMed: 20135094]

27. Ma YL, Bryant HU, Zeng Q, Schmidt A, Hoover J, Cole HW, et al. New bone formation with teriparatide [human parathyroid hormone-(1-34)] is not retarded by long-term pretreatment with alendronate, estrogen, or raloxifene in ovariectomized rats. Endocrinology. May; 2003 144(5): 2008–15. Epub 2003/04/17. [PubMed: 12697709]

28. Amugongo SK, Yao W, Jia J, Lay YA, Dai W, Jiang L, et al. Effects of sequential osteoporosis treatments on trabecular bone in adult rats with low bone mass. Osteoporos Int. Jun; 2014 25(6): 1735–50. Epub 2014/04/12. [PubMed: 24722767]

29. Altman AR, Tseng WJ, de Bakker CM, Huh BK, Chandra A, Qin L, et al. A closer look at the immediate trabecula response to combined parathyroid hormone and alendronate treatment. Bone. Jan 24.2014 61C:149–57.

30. De Bakker CM, Altman AR, Tseng WJ, Tribble MB, Li C, Chandra A, et al. μCT-based, in vivo dynamic bone histomorphometry allows 3D evaluation of the early responses of bone resorption and formation to PTH and alendronate combination therapy. Bone. 2015; 73:198–207. [PubMed: 25554598]

31. Lan S, Luo S, Huh BK, Chandra A, Altman AR, Qin L, et al. 3D image registration is critical to ensure accurate detection of longitudinal changes in trabecular bone density, microstructure, and stiffness measurements in rat tibiae by in vivo micro computed tomography (μCT). Bone. 2013; 56(1):83–90. [PubMed: 23727434]

32. de Bakker CM, Altman AR, Li C, Tribble MB, Lott C, Tseng WJ, et al. Minimizing interpolation bias and precision error in *in vivo* microCT-based measurements of bone structure and dynamics.

Annals of biomedical engineering. Jan 19; 2016 44(8):2518–28. Epub 2016/01/21. [PubMed: 26786342]

33. Bach-Gansmo FL, Irvine SC, Bruel A, Thomsen JS, Birkedal H. Calcified cartilage islands in rat cortical bone. Calcif Tissue Int. Apr; 2013 92(4):330–8. [PubMed: 23274728]
34. Collignon, A., Maes, F., Delaere, D., Vandermeulen, D., Suetens, P., Marchal, G. Automated multi-modality image registration based on information theory. In: Bizais, Y.Barillot, C., di Paola, R., editors. Information Processing in Medical Imaging. Kluwer Academic Publishers; Dordrecht, The Netherlands: 1995. p. 263-274.
35. Viola P, Wells WM III. Alignment by maximization of mutual information. International Journal of Computer Vision. 1997; 24(2):137–54.
36. Ibanez, L., Schroeder, W., Ng, L., Cates, J. [Accessed May 11, 2016. 2005] The ITK Software Guide. 2Available at http://wwwitkorg/ItkSoftwareGuidepdf
37. Parfitt AM, Drezner MK, Glorieux FH, Kanis JA, Malluche H, Meunier PJ, et al. Bone histomorphometry: standardization of nomenclature, symbols, and units. Report of the ASBMR Histomorphometry Nomenclature Committee. J Bone Miner Res. Dec; 1987 2(6):595–610. [PubMed: 3455637]
38. Saha PK, Chaudhuri BB, Chanda B, Dutta Majumder D. Topology preservation in 3D digital space. Pattern Recogn. 1994; 27:295–300.
39. Saha PK, Chaudhuri BB, Majumder DD. A new shape preserving parallel thinning algorithm for 3D digital images. Pattern Recogn. 1997; 30(12):1939–55.
40. Liu XS, Sajda P, Saha PK, Wehrli FW, Guo XE. Quantification of the roles of trabecular microarchitecture and trabecular type in determining the elastic modulus of human trabecular bone. J Bone Miner Res. Oct; 2006 21(10):1608–17. [PubMed: 16995816]
41. Schriefer JL, Robling AG, Warden SJ, Fournier AJ, Mason JJ, Turner CH. A comparison of mechanical properties derived from multiple skeletal sites in mice. J Biomech. Mar; 2005 38(3): 467–75. Epub 2005/01/18. [PubMed: 15652544]
42. Pendleton, MM., Alwood, JS., O'Connell, GD., Keaveny, TM. Design of fatigue test for ex-vivo mouse vertebra. Summer Biomechanics, Bioengineering and Biotransport Conference; National Harbor, MD. 2016;
43. Kim DG, Huja SS, Lee HR, Tee BC, Hueni S. Relationships of viscosity with contact hardness and modulus of bone matrix measured by nanoindentation. J Biomech Eng. Feb.2010 132(2):024502. Epub 2010/04/08. [PubMed: 20370248]
44. Kim DG, Huja SS, Navalgund A, D'Atri A, Tee B, Reeder S, et al. Effect of estrogen deficiency on regional variation of a viscoelastic tissue property of bone. J Biomech. Jan 4; 2013 46(1):110–5. Epub 2012/11/13. [PubMed: 23141522]
45. Huja SS, Beck FM, Thurman DT. Indentation properties of young and old osteons. Calcif Tissue Int. Jun; 2006 78(6):392–7. Epub 2006/07/11. [PubMed: 16830198]
46. Oliver WC, Pharr GM. An improved technique for determining hardness and elastic modulus using load and displacement sensing indentation experiments. J Mater Res. 1992; 7(6):1564–83.
47. Canalis E, Giustina A, Bilezikian JP. Mechanisms of anabolic therapies for osteoporosis. N Engl J Med. Aug 30; 2007 357(9):905–16. [PubMed: 17761594]
48. Sengupta P. The Laboratory Rat: Relating Its Age With Human's. Int J Prev Med. Jun; 2013 4(6): 624–30. [PubMed: 23930179]
49. Altman A, de Bakker CM, Tseng WJ, Chandra A, Qin L, Liu XS. Enhanced Individual Trabecular Repair and Its Mechanical Implications in PTH and Alendronate Treated Rat Tibial Bone. J Biomech Eng. Oct 1.2015 137(1):011004-1-8. Epub 2014/10/17.
50. Rubin MR, Bilezikian JP. The anabolic effects of parathyroid hormone therapy. Clin Geriatr Med. May; 2003 19(2):415–32. [PubMed: 12916294]
51. Tai K, Dao M, Suresh S, Palazoglu A, Ortiz C. Nanoscale heterogeneity promotes energy dissipation in bone. Nat Mater. Jun; 2007 6(6):454–62. Epub 2007/05/23. [PubMed: 17515917]
52. Renders GA, Mulder L, van Ruijven LJ, Langenbach GE, van Eijden TM. Mineral heterogeneity affects predictions of intratrabecular stress and strain. J Biomech. Feb 03; 2011 44(3):402–7. [PubMed: 21040918]

53. Goff MG, Slyfield CR, Kummari SR, Tkachenko EV, Fischer SE, Yi YH, et al. Three-dimensional characterization of resorption cavity size and location in human vertebral trabecular bone. Bone. Apr 3; 2012 51(1):28–37. [PubMed: 22507299]

54. Slyfield CR, Tkachenko EV, Wilson DL, Hernandez CJ. Three-dimensional dynamic bone histomorphometry. J Bone Miner Res. Feb; 2012 27(2):486–95. [PubMed: 22028195]

55. Klinck RJ, Campbell GM, Boyd SK. Radiation effects on bone architecture in mice and rats resulting from in vivo micro-computed tomography scanning. Med Eng Phys. Sep; 2008 30(7): 888–95. [PubMed: 18249025]

56. Brouwers JE, van Rietbergen B, Huiskes R. No effects of in vivo micro-CT radiation on structural parameters and bone marrow cells in proximal tibia of wistar rats detected after eight weekly scans. J Orthop Res. Oct; 2007 25(10):1325–32. [PubMed: 17568420]

57. Willett TL, Pasquale J, Grynpas MD. Collagen modifications in postmenopausal osteoporosis: advanced glycation endproducts may affect bone volume, structure and quality. Current osteoporosis reports. Sep; 2014 12(3):329–37. Epub 2014/06/02. [PubMed: 24880722]

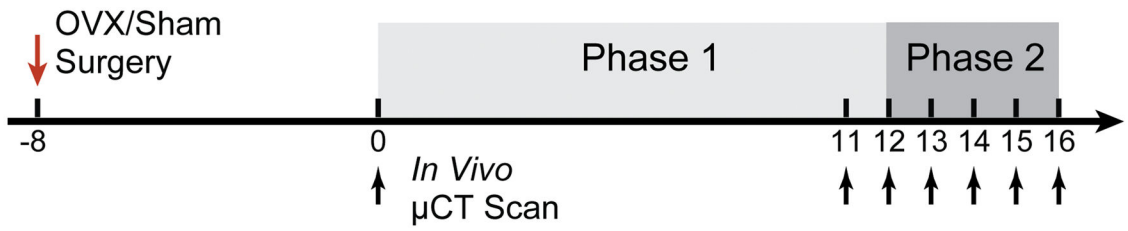


| | Surgery | Phase 1 | | | Phase 2 |
|---|---|---|---|---|---|
| Group | Week -8 | 0-4 | 4-8 | 8-12 | 12-16 |
| **SHAM** | Sham | ← **No Treatment** → | | | |
| **VEH** | OVX | ← **VEH** → | | | **VEH** |
| **VEH/PTH** | OVX | ← **VEH** → | | | **PTH** |
| **ALN** | OVX | ← **ALN** → | | | **ALN** |
| **ALN/PTH** | OVX | ← **ALN** → | | | **PTH** |

**Figure 1.**
Schematics of surgery and treatment strategies.

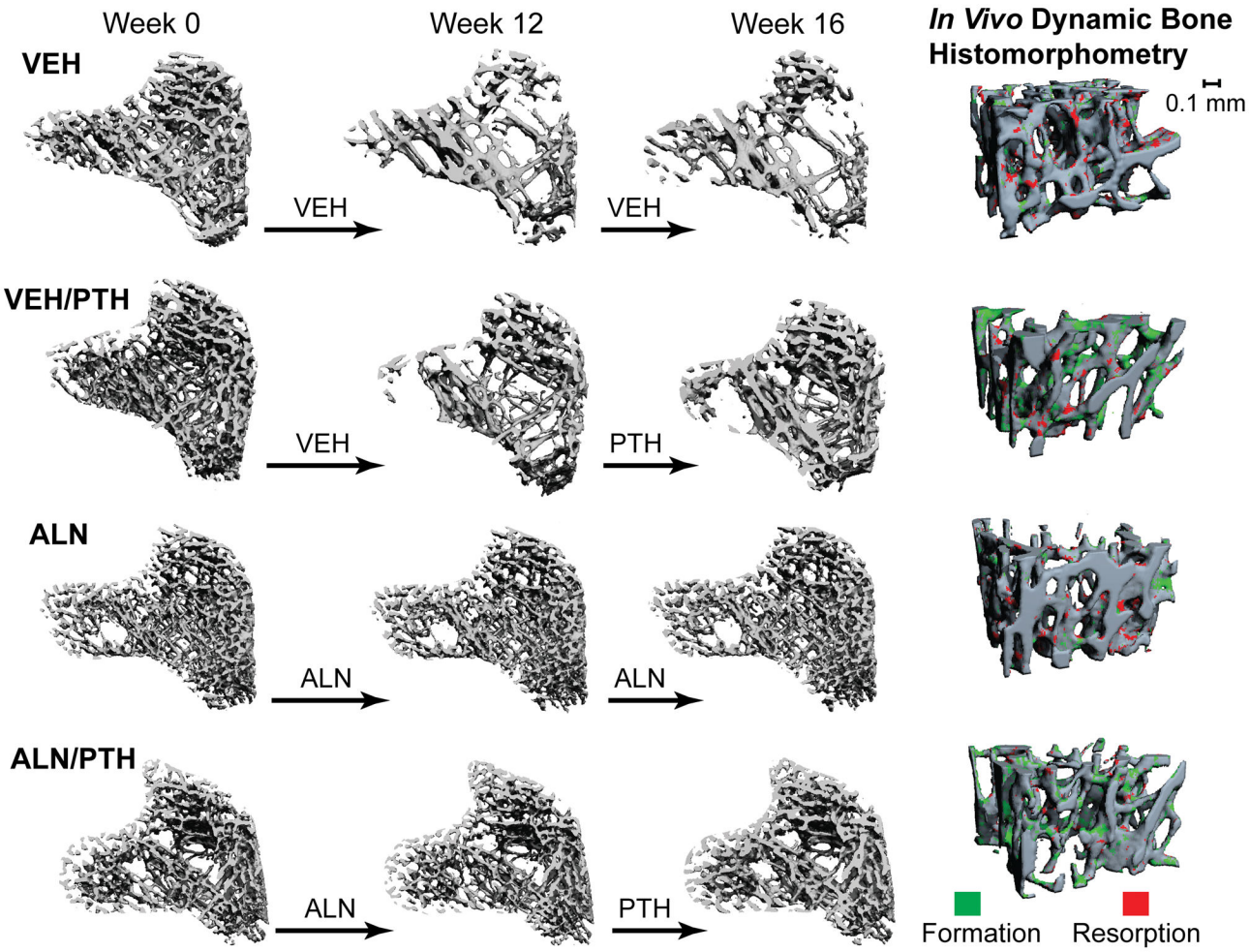


**Figure 2.**

Left: Registered comparison of tibia bone segments at week 0, 12, and 16 with treatment indicated by the arrows between time points. Right: 3D *in vivo* bone dynamic histomorphometry. Green indicates areas of new bone formation, and red indicates areas of bone resorption during the final week of treatment (week 15–16).

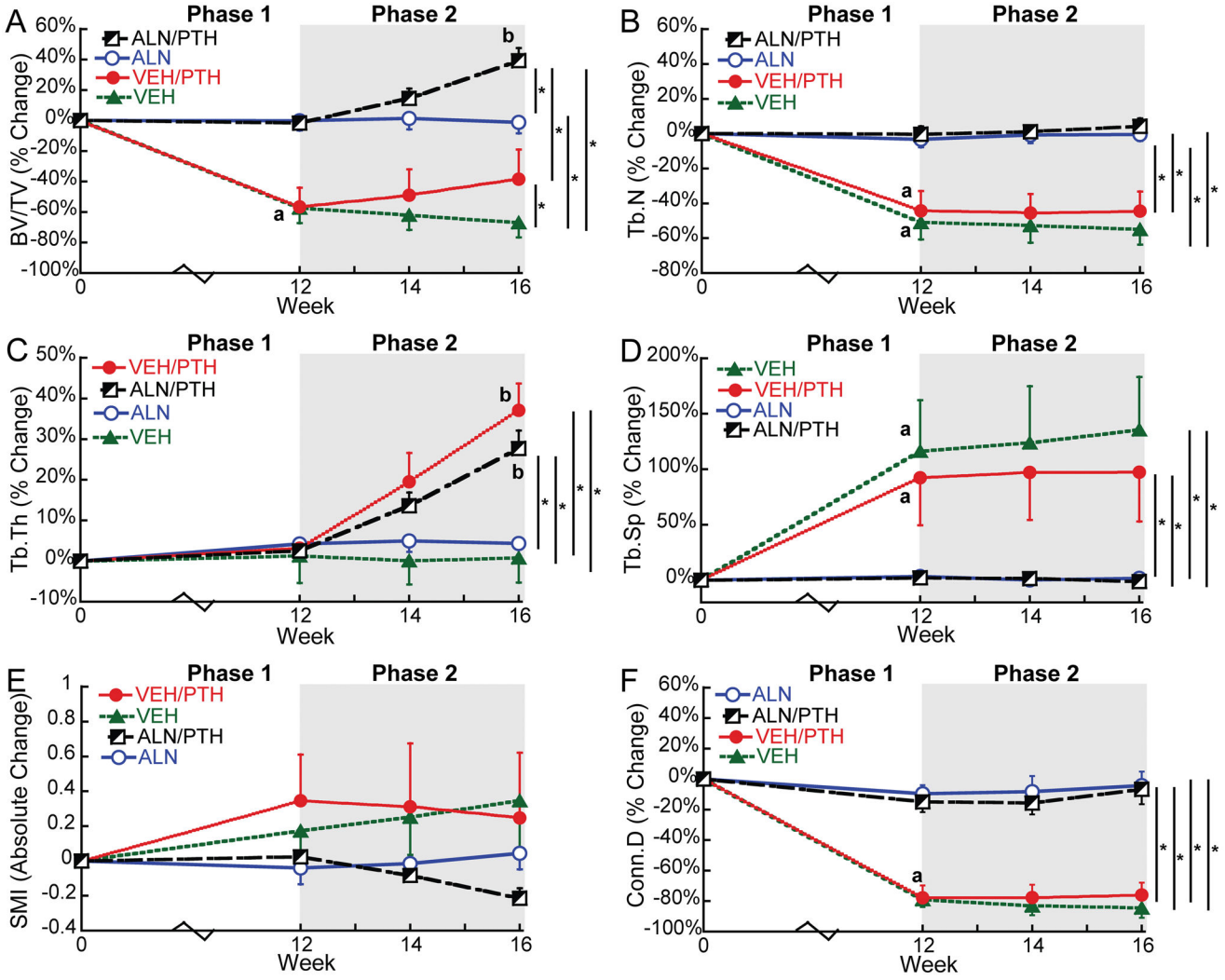


**Figure 3.**

Percent changes (Mean±SD) from baseline in the tibial trabecular bone microstructure in response to OVX and treatments. Letters indicate significant change from baseline (a) or week 12 (b). * indicates a significant difference between groups.

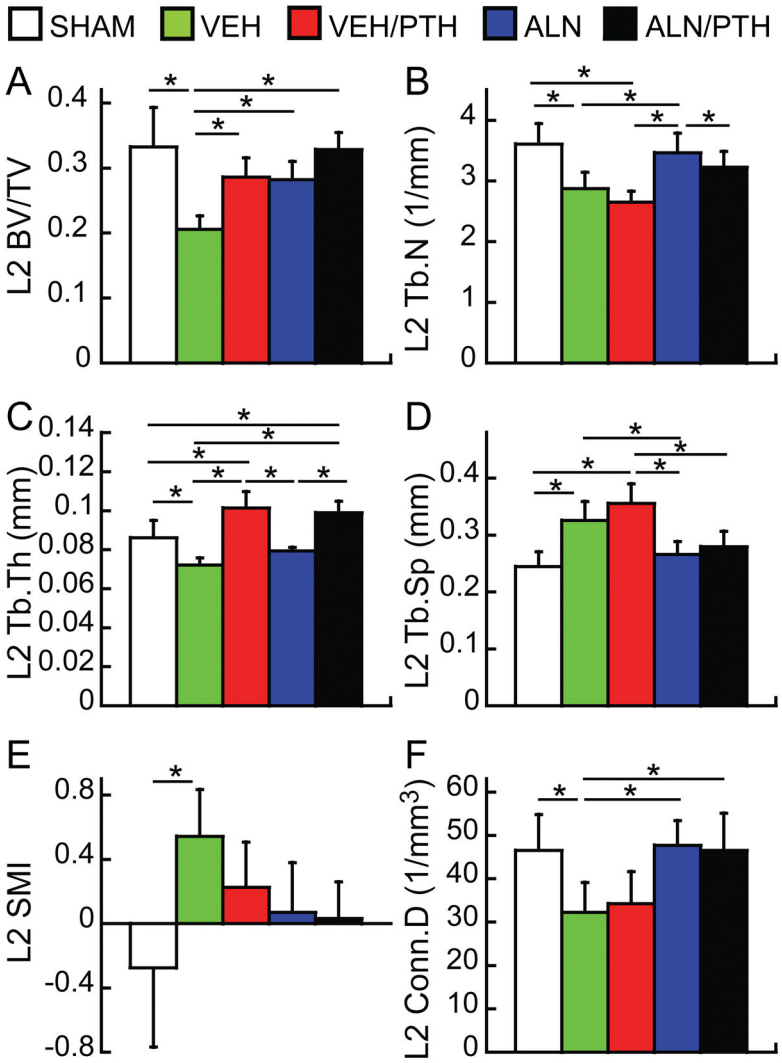


**Figure 4.**

Comparisons between treatment groups at the end of Phase 2 treatment (week 16) in trabecular bone microstructure of lumbar vertebra L2. * indicates a significant difference between groups ($p<0.05$).

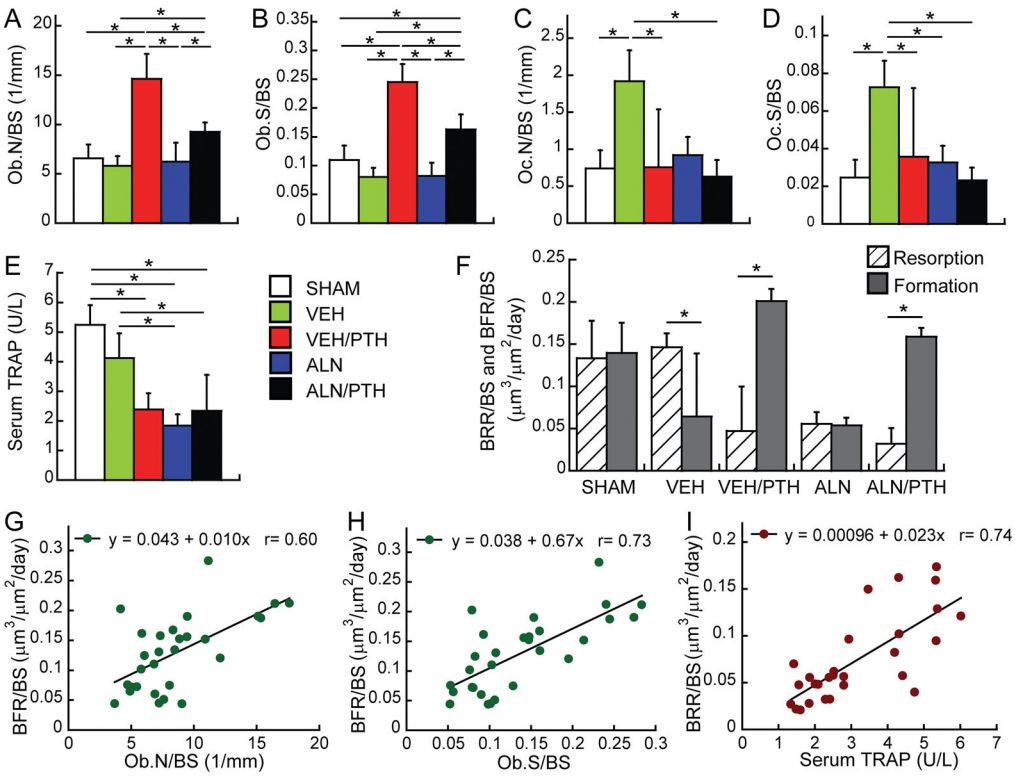


**Figure 5.**

(A–E) Comparisons between treatment groups at the end of Phase 2 treatment (week 16) in static bone histomorphometry parameters of the proximal tibia and serum TRAP level. * indicates a significant difference between treatment groups. (F) Bone resorption rate (hashed bar) and formation rate (solid bar) of the proximal tibia estimated by 3D *in vivo* dynamic bone histomorphometry. * indicates a significant difference between resorption and formation. (G–I) Linear correlations between 2D static histomorphometry/serum analysis parameters and 3D *in vivo* bone dynamic parameters.

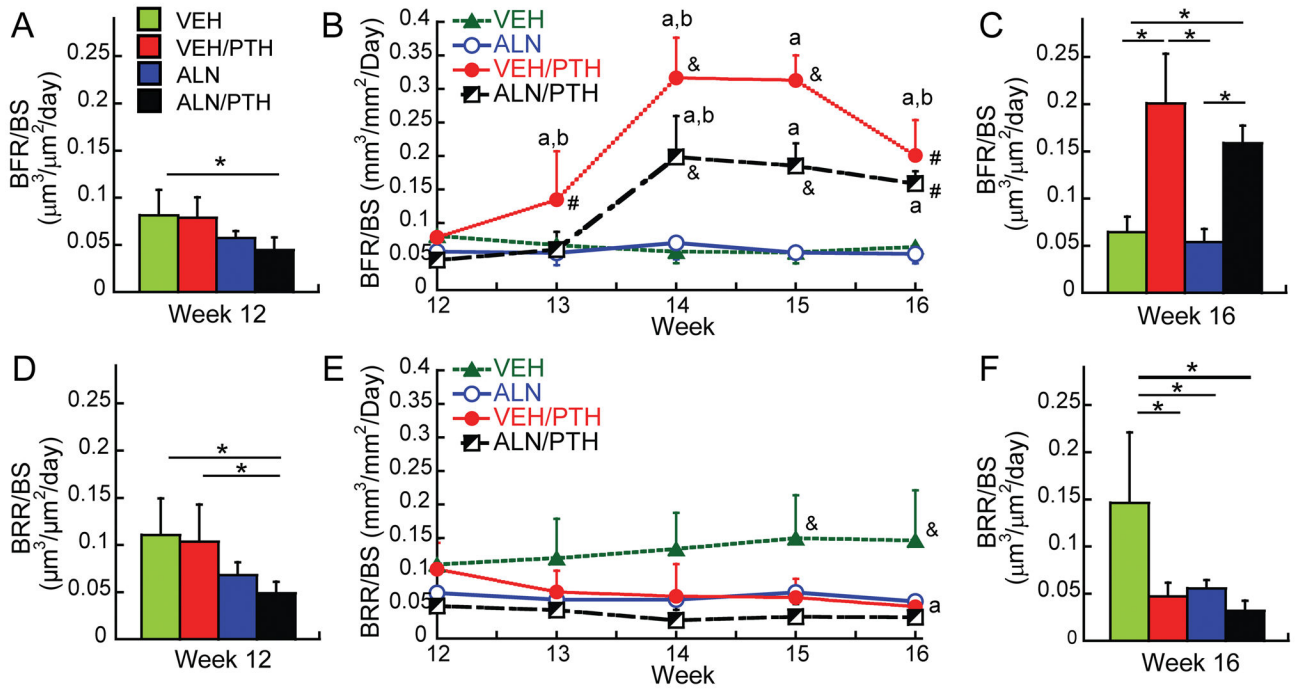


**Figure 6.**

(Left and right panels) group comparisons in bone formation rate (BFR/BS) and bone resorption rate (BRR/BS) at the beginning of the Phase 2 treatment (week 12, A&D) and the end of Phase 2 (week 16, C&F); * indicates a significant difference between treatment groups. (Middle panel) longitudinal changes in (B) BFR/BS and (E) BRR/BS of each treatment group during the Phase 2. [a] significant difference from week 12; [b] significant difference from the previous week; [#] significant difference from VEH and ALN groups; [&] significant difference from all other groups.

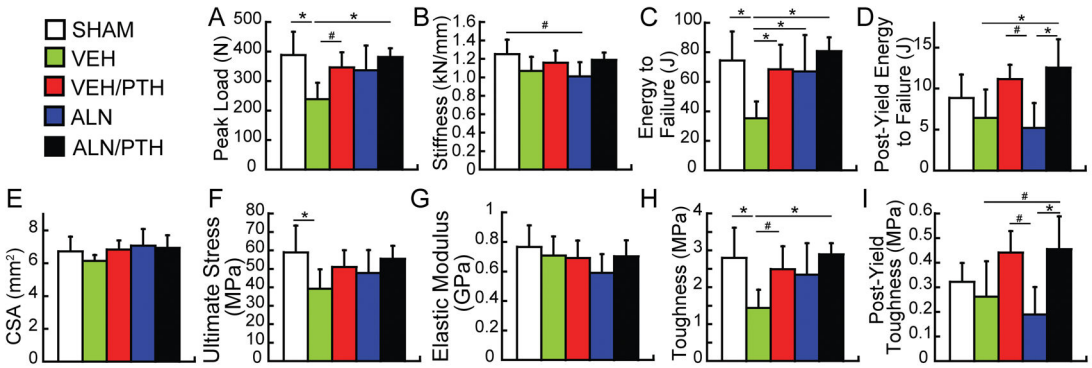


**Figure 7.**

Comparisons between treatment groups at the end of Phase 2 treatment (week 16) in mechanical properties of lumbar vertebra L1. * significant difference between groups ($p<0.05$) # trend toward difference between groups ($p<0.1$).

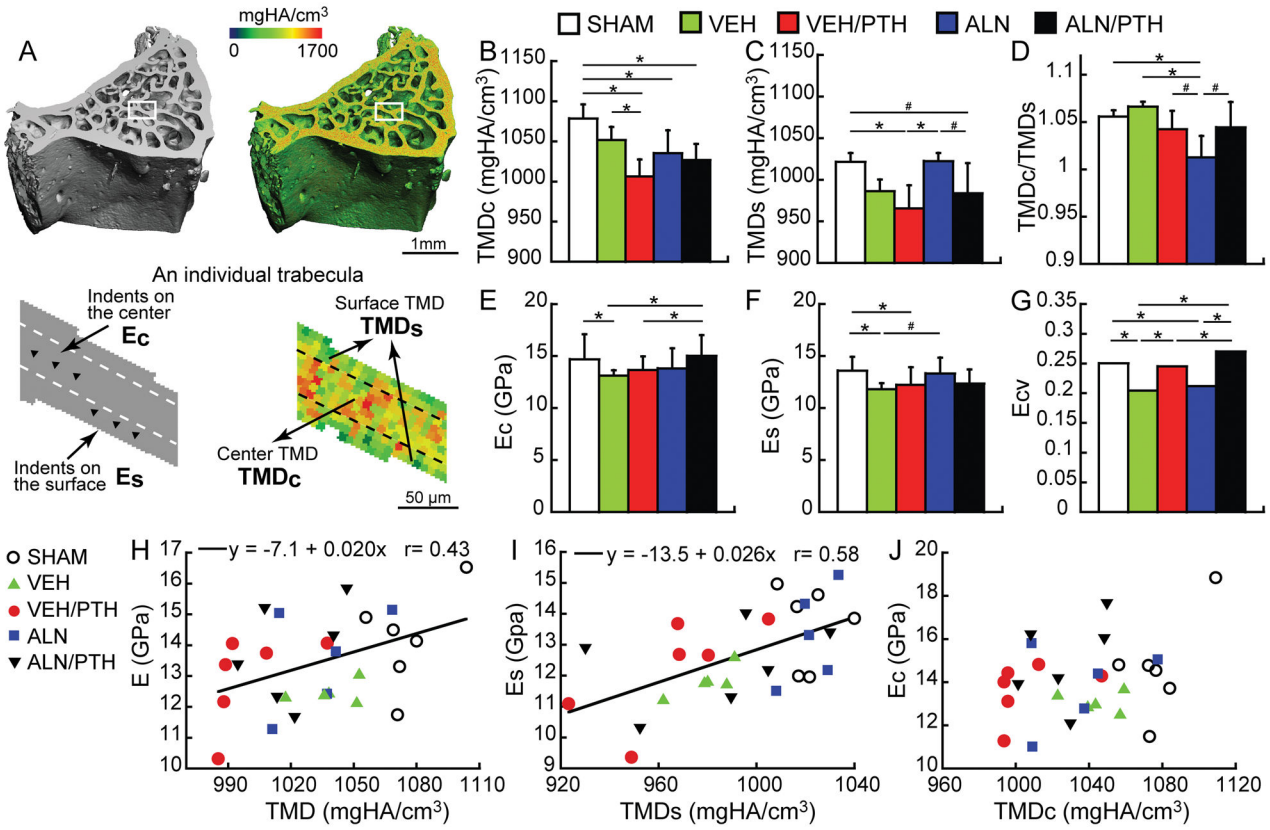


**Figure 8.**

(A) Schematics of TMD and E measurements at the center and surface of individual trabeculae. (B–D) Comparisons in the center, surface, and center-to-surface ratio of TMD measurements between treatment groups. (E–G) Comparisons in the center, surface, and variance of elastic modulus by nano indentation between treatment groups. (H–I) Correlations between tissue mineral density (TMD, TMDs, and TMDc) and tissue elastic modulus (E, Es, and Ec). * significant difference between groups ($p<0.05$) # trend toward difference between groups ($p<0.1$).